

# A stable, accurate, and efficient approach to explicit depth migration

Gary F. Margrave, Hugh D. Geiger, Saleh M. Al-Saleh, and Michael P Lamoureux, University of Calgary

2005 CSEG National Convention



## Summary

We present a new approach to the design of stable and accurate wavefield extrapolation operators needed for explicit depth migration. We split the theoretical operator into two component operators, one a forward operator that controls the phase accuracy and the other an inverse operator, designed as a Wiener filter, that stabilizes the first operator. Both component operators are designed to have a specific fixed length and the final operator is formed as the convolution of the components. We utilize this operator design method to build an explicit, wavefield extrapolation method based on the migration of individual source records. Two other features of our method are the use of dual operator tables, with high and low levels of evanescent filtering, and frequency-dependent spatial down sampling. Both of these features improve the accuracy and efficiency of the overall method. Empirical testing shows that our method has a similar performance to the time-migration method called phase shift, meaning it scales as  $N \log N$ . We illustrate the method with tests on the Marmousi synthetic dataset. We call our method *FOCI* which is an acronym for *forward operator conjugate inverse*.

## Introduction

We begin with a 2D wavefield  $y(x, z, w)$  which has already been Fourier transformed over the temporal coordinate. Then wavefield extrapolation in the space-frequency domain can be expressed as a spatial convolution given by

$$y(x, z + Dz, w) = \int_{\square} y(u, z, w) W(x - u, k(x), Dz) du \quad (1)$$

where  $u$  denotes the transverse spatial coordinates at input and

$$W(x - u, k(x), Dz) = \frac{1}{2p} \int_{\square} \hat{W}(k_x, k(x), Dz) e^{-ik_x(x-u)} dk_x \quad (2)$$

with

$$\hat{W}(k_x, k(x), Dz) = \exp\left\{ \frac{Dz}{\vartheta} \sqrt{k(x)^2 - k_x^2} \right\} \quad (3)$$

and

$$k(x) = \frac{w}{v(x)} \quad (4)$$

For constant velocity, equation (1) is the space-frequency domain equivalent to the phase shift method, while for variable velocity, it is equivalent to the GPSP (generalized phase shift plus interpolation) of Margrave and Ferguson (1999). When applied directly, equation (1) is very expensive because the operator  $W$  in equation (2) does not have compact support (i.e. it is infinite in spatial extent). A fast and efficient wavefield extrapolation scheme can be developed from equation (1) if  $W$  can somehow be localized; that is if a stable, compactly supported approximation,  $\tilde{W}$ , can be found. It is well established (e.g. Hale 1991) that most simple localizations such as windowing lead to unstable operators. Here, instability means that, when equation (1) is applied repeatedly in a wavefield extrapolation process, the wavefield amplitude grows uncontrollably. To understand this effect, note that  $|\hat{W}| = 1, k^2 > k_x^2$  (wavelike) while  $\hat{W} = \exp(-z|k_z|) < 1, k^2 > k_x^2$  (evanescent). A windowing operation is a convolution of the operator and the window in the wavenumber domain and most compactly supported window choices cause  $|\hat{W}|$  to fluctuate slightly from the desired value of unity in the wavelike region. Suppose  $|\hat{W}| = 1 + e, k^2 > k_x^2$  where  $|e| < 1$ , then the application of this operator in  $m$  recursive steps results in  $|\hat{W}^m| = (1 + e)^m \gg 1 + me$ . In the subsequent discussion, all operator designs will have nonzero  $e$  and so are technically unstable. However, we will say an operator is practically stable for  $m$  steps if  $|\hat{W}^m| \gg 1 + me < 1.2$  where 1.2 represents an arbitrary 20% tolerance. For example, if a depth migration is to be run with 10m steps to a depth of 5000m, then we require stability for  $m = 500$  steps. We infer that we must have  $|e| < .2/500 = .0004$ . Thus we can tolerate a  $\hat{W}$  whose absolute value in the wavelike region departs from unity by not more than 4 parts in 10,000.

## A stabilizing Wiener filter and the FOCI extrapolator

First we point out two useful properties of  $\hat{W}$ :

$$\hat{W}(k_x, k, Dz) = \hat{W}^* \left( k_x, k, \frac{Dz}{\vartheta} \right) \quad \text{and} \quad \hat{W}^{-1}(k_x, k, Dz) = \hat{W}^*(k_x, k, Dz), \quad k^2 > k_x^2 \quad (5)$$

where the  $*$  indicates the complex conjugate. Next, let  $\tilde{W}(Dz/2)$  be any compactly supported approximate wavefield extrapolator (where we have suppressed all functional dependence except  $Dz$ ). Then we seek another compactly supported operator,  $\tilde{W}_I$ , such that

$$\tilde{W}_I \cdot \tilde{W}(Dz/2) = F^{-1} \left\{ \tilde{W}(Dz/2) \right\}^h \Big|_{\tilde{u}} \quad (6)$$

where  $0 \leq h \leq 2$  is an adjustable parameter and  $F^{-1}$  symbolizes the inverse Fourier transform. The function of the right hand side of equation (6) is a zero-phase, band-limited approximation to a delta function. If  $h = 0$  it is truly a delta function and hence  $\tilde{W}_I$  will be an inverse of  $\tilde{W}(Dz/2)$ . When  $h > 0$ ,  $\tilde{W}_I$  will be a band-limited inverse of  $\tilde{W}(Dz/2)$ . Since  $\tilde{W}(Dz/2)$  has half the phase of  $\tilde{W}(Dz)$ , and since  $\tilde{W}_I$  has the negative of the phase of  $\tilde{W}(Dz/2)$  (regardless of the value of  $h$ ), we form the FOCI approximation to  $W(Dz)$  as

$$W_F(Dz) = \tilde{W}_I^* \cdot \tilde{W}(Dz/2) \gg W(Dz) \quad (7)$$

which follows from the approximate inverse nature of  $\tilde{W}_I$  and from equations (5). As equation (7) shows, the FOCI operator is formed from the convolution of an approximate forward operator with the conjugate of its bandlimited inverse, hence the acronym FOCI. Since both  $\tilde{W}(Dz/2)$  and  $\tilde{W}_I$  are compactly supported (by design) then so is  $W_F$ .

Equation (6) is easily solved exactly in the Fourier domain, but the resulting  $\tilde{W}_I$  will not have compact support. Therefore we solve the discrete equivalent of equation (6) in the least-squares sense seeking a  $\tilde{W}_I$  with specific compact support. Then  $W_F$  will also have compact support that will be the sum of the supports of  $\tilde{W}(Dz/2)$  and  $\tilde{W}_I$ . Equation (6) poses  $\tilde{W}_I$  as a Wiener least-squares filter that matches  $\tilde{W}(Dz/2)$  to a particular bandlimited impulse.

Some general features of this scheme are

- The phase accuracy is limited by the initial estimate of the forward operator for a half-step,  $\tilde{W}(Dz/2)$ .
- Stability is generally enhanced by a longer  $\tilde{W}_I$ . A good choice for  $m = \text{length}(\tilde{W})$  is  $m^3 \approx 3p/2$ .
- The parameter  $h$  (equation (6)) controls the degree of evanescent filtering in the final composite operator  $W_F$  (equation (7)). Larger values of  $h$  give operators that are less stable than those arising from smaller values. For  $h = 0$ , the resulting  $W_F$  is all-pass (no evanescent filtering), while for  $h = 2$ ,  $W_F$  has the full evanescent filtering expected from theory.
- The length of  $W_F$  in samples, is given by  $n_{op} = n_{for} + n_{inv} - 1$  where  $n_{for} = \text{length}(\tilde{W})$  and  $n_{inv} = \text{length}(\tilde{W}_I)$ .

### Dual operator tables for increased stability

Since evanescent filtering contributes to operator instability, it is natural to ask if it is required. Certainly, for a marching scheme in constant velocity, only the first few applications of the evanescent filter make any difference to the final result. This is because the wavenumber defining the evanescent boundary,  $k_{ev} = \pm w/v$ , does not change. It follows that repeated applications of the evanescent filter in a constant velocity scenario only cause reduced stability. For the inhomogeneous case, we expect that it is similarly not necessary to apply the full evanescent filter on every step. Therefore, we construct two operator tables for use in any depth migration, a first table with strong evanescent filtering and a second with very little. This corresponds to the choice of two different  $h$  values (equation (6)) when constructing these tables. Then, for most extrapolation steps we use the second table corresponding to a small  $h$ , but for every  $j^{\text{th}}$  step, we use the first table with large  $h$ .

### Spatial resampling

Most wavefield-extrapolation, depth-migration schemes use a fixed operator length that is independent of frequency. In general, as frequency decreases, an operator of fixed size becomes increasingly problematic. Let  $Dx$  be the spatial sample size, then the Nyquist wavenumber is  $k_{nyq} = p/Dx$  while the evanescent boundary is at  $k_{ev} = w/v$ . Since the spatial sample interval for an  $n_{op}$ -length wavefield extrapolator is also  $Dx$ , and assuming that  $n_{op}$  is an odd number, the Fourier transform of the operator will have samples at wavenumbers  $k_{xop} = Dk(0, \pm 1, \pm 2, \dots, \pm (n_{op} - 1)/2)$  where  $Dk = 2p/(n_{op}Dx)$ . That is, the operator has a sample at 0 wavenumber and then  $(n_{op} - 1)/2$  samples distributed out to just shy of  $+k_{nyq}$  in the positive wavenumber band and similarly for the negative wavenumbers. Thus, while the data may have hundreds of wavenumbers below  $k_{ev}$ , the operator may have only a few, or in the worst case only one (at zero), such wavenumbers. This becomes increasingly likely as frequency decreases or velocity increases. Thus a migration conducted with a fixed operator length, where typically  $n_{op}$  is a number like 21 or 31, will have many circumstances where most of the operator wavenumbers fall in the evanescent region. Such operators have poor phase control and are relatively unstable. As a solution, we advocate spatially resampling of the data at lower frequencies to a sample rate  $Dx \ll Dx$ . We break the  $[w_{min}, w_{max}]$  frequency band into frequency "chunks",  $n_{chunk}$  in number, and spatially resample the  $j^{\text{th}}$  chunk from  $Dx$  to  $Dx_j > Dx$  such that  $a p / Dx_j \leq w / v_{crit} \leq b p / Dx_j$ ,  $a < b \hat{1} [0,1]$  where  $v_{crit}$  is a velocity chosen to define the highest

evanescent boundary of interest. A good, and always sufficient, choice for  $v_{crit}$  is  $v_{crit} = \min(v(x_T, z))$ , that is use the minimum velocity found anywhere in the velocity model. In our testing to date, we take  $a = .7$  and  $b = .9$ . Specifying  $a$  and  $b$  determines the value of  $nchunk$  which typically is near 10. Thus we are always assured that at least 70% of the wavenumber samples of the operator fall within the wavelike region.

Since we are resampling to a coarser sample rate an anti-alias filter is required to avoid aliasing. The algorithm used for spatial resampling is important since we want to preserve data at the highest wavelike wavenumbers without any loss and utterly reject anything that is evanescent. Furthermore, we cannot tolerate ripples in the passband. The obvious choice is a truncation operation in the wavenumber domain where data at all wavenumbers greater than the new Nyquist are rejected and data at wavenumbers greater than  $w/v_{crit}$  are zeroed. If the data has  $n$  spatial locations before resampling and  $m_j < n$  wavenumbers are retained after resampling, it can be shown that the resulting spatial sample interval will be  $Dx_j = Dx(n/m_j)$  so the new sample interval is formed from the original by multiplication by a rational number.

At this time, we conduct spatial resampling only once at the beginning of the downward extrapolation process. Thus the resampling is determined by the shallow part of the velocity model because that is where the lowest velocities are found. In principle, it would be beneficial to repeat the resampling periodically during the downward continuation process. Once resampled, we preserve the data in these frequency chunks with their differing sample rates during the entire process. Since a typical imaging condition requires a summation over frequency, we restore the original sample interval in the application of the imaging condition at each depth.

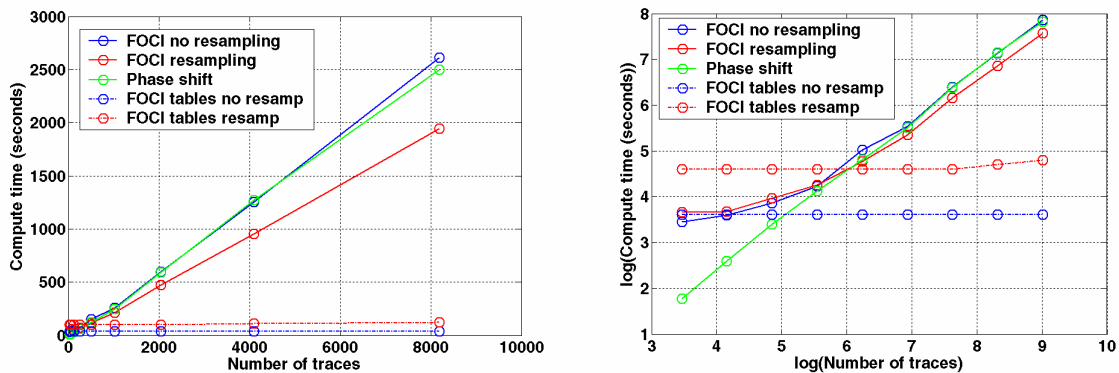


Figure 1: Time trials comparing the runtimes for FOCI with and without spatial resampling and the runtimes of the time migration algorithm called phase shift. (Left) FOCI depth migration and phase shift time migration are seen to have similar run times over nearly three orders of magnitude of dataset size. Spatial resampling is seen cause about a 20% speedup. (Right) The same data plotted on a log-log scale show all three algorithms with slope near unity for large  $N$  which indicates  $N \log N$  scaling.

## Time trials and Marmousi Images

We have also conducted time trials of the FOCI algorithm with and without spatial resampling and, for comparison, we also used the phase-shift algorithm. Of course, phase-shift is only a time migration method while FOCI is a depth migration but the former is well known to show  $N \log N$  scaling (where  $N$  is the number of points in the dataset) so it is a good point of comparison. All of these algorithms were post-stack implementations. To conduct these tests, we generated a sequence of nine datasets with the number of traces starting at 32 and doubling each time until the ninth dataset which had 8192 traces. Thus we have scanned over two orders of magnitude of dataset size. Figure 1 (left) plots the resulting run times on a 2.5 GHz PC (with 2 GB memory) versus the number of traces, while Figure 1 (right) shows these same data on a log-log scale. From Figure 3, we can see that FOCI without spatial down-sampling appears to be as fast as phase shift and that spatial down-sampling appears to speed up FOCI by about 20%. The conclusion that FOCI with spatial down-sampling is faster than phase shift is certainly dependent upon our phase-shift code. While we are confident that our phase-shift algorithm is well written, it uses the standard practice of explicitly calculating the phase-shift operator at each depth step. Certainly precalculating the phase-shift operators and storing them in a table would result in a faster algorithm. The 20% speedup due to spatial resampling is an unambiguous observation. We expect greater speedups in 3D.

We have conducted a series of tests of the FOCI algorithm in imaging the Marmousi structure with pre-stack depth migration. The Marmousi dataset (Bourgeois et al., 1991) is a 2D, acoustic, finite-difference model created over a very complex structure (Figure 2, left) and has been widely used to test imaging algorithms. The dataset consists of 240 individual shot records of 96 traces each in a marine, towed streamer, configuration. The source and receiver intervals are 25 m and the highest coherent frequencies to be found are about 50 Hz. Prior to migration, we applied a wavelet shaping filter designed to whiten the signal spectrum and interpolated each

shot to a receiver spacing of 12.5 m. Figure 2 (right) is a prestack depth migration (a stack of individually migrated shot records) using a 51 point FOCI operator. Comparison shows that FOCI has resolved virtually the entire section and verifies that our algorithm is sufficiently stable and accurate for this task. This migration required about 23 hours on a single 2.5 GHz PC. Using shorter operators and coarser spatial sampling, we have obtained useful prestack depth images of Marmousi in as little as one hour.

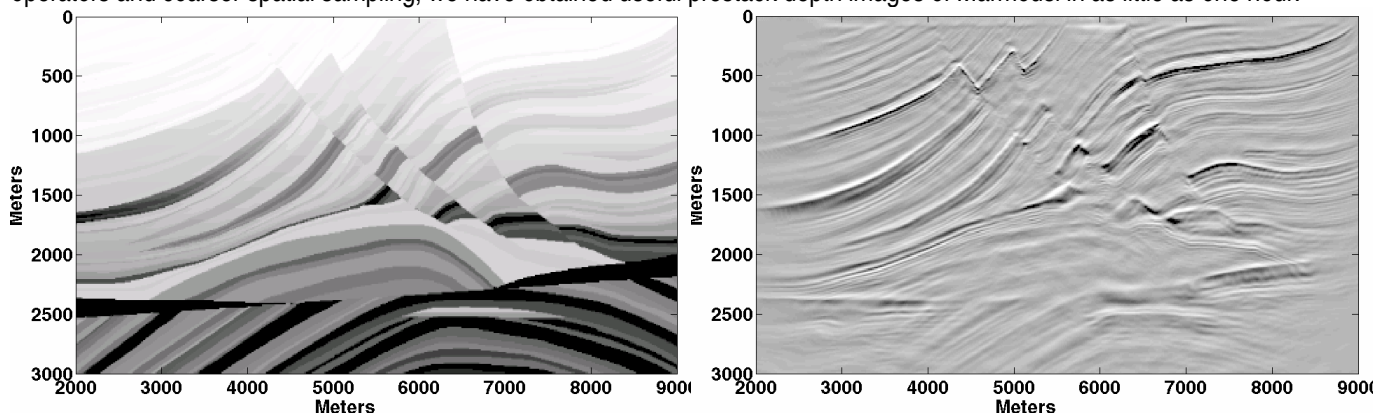


Figure 2. (Left) The Marmousi velocity model with dark shading indicating faster velocities. (Right) A prestack depth migration result using a 51 point operator designed with the FOCI algorithm.

## Conclusion

We have presented a new algorithm for constructing a compactly supported, explicit, space-frequency domain depth migration operator. The operator is designed by first truncating the exact operator for a half-depth-step to a desired length and then designing a fixed-length, least-squares, band-limited inverse for the truncated operator. The final FOCI operator is formed from the convolution of the forward operator with the conjugate of its band-limited inverse. We have demonstrated that this operator can be constructed with good stability and phase accuracy. We have then implemented pre and post-stack explicit depth migrations with this operator design. Significant innovations in our depth migration algorithms are the use of dual operator tables, with low and high levels of evanescent filtering, and spatial down-sampling of the lower frequencies. These innovations increase operator accuracy and stability as well as shorten the overall computation time. Testing of this algorithm shows that it scales approximately as order  $N \log N$  over at least three orders of magnitude of dataset size. Excellent images are now being obtained with both pre and post-stack depth migration.

## Acknowledgements

We thank the industrial sponsors of both the Consortium for Research in Elastic Wave Exploration Seismology (CREWES) and the Pseudodifferential Operator Theory in Seismic Imaging (POTS) project. We also thank the Canadian organizations: Natural Sciences and Engineering Research Council (NSERC), the Mathematics of Information Technology and Complex Systems network of centres of excellence (MITACS), and the Pacific Institute for the Mathematical Sciences (PIMS) for their funding assistance.

## Notice of Patent Application

A US patent application describing a unique FOCI™ process is being considered and is currently in the due diligence stage. The patent application will be drafted to contain language and claims describing the design of a stable operator by the forward-operator-conjugate-inverse method, the use of dual operator tables to reduce evanescent filtering, and spatial down-sampling as a method to increase operator performance and reduce computation time.

## References

- Bourgeois, A., Bourget, M., Lailly, P., Poulet, M., Ricarte, P. and Versteeg, R., 1991, Marmousi, model and data: in Versteeg, R. and Grau, G. (editors), 1991, The Marmousi experience, proceedings of the 1990 EAGE workshop on practical aspects of seismic data inversion, EAGE, p5-16.
- Hale, D., 1991, Stable explicit extrapolation of seismic wavefields: *Geophysics*, 56, 1770–1777.
- Margrave, G. F. and Ferguson, R. J., 1999, Wavefield extrapolation by nonstationary phase shift: *Geophysics*, 64, 1067-1078.